



Atomic loss and gain as a resource for nonequilibrium phase transitions in optical lattices

B. Everest, M. Marcuzzi, and I. Lesanovsky

School of Physics and Astronomy, The University of Nottingham, Nottingham NG7 2RD, United Kingdom

(Received 28 July 2015; published 9 February 2016)

Recent breakthroughs in the experimental manipulation of strongly interacting atomic Rydberg gases in lattice potentials have opened an avenue for the study of many-body phenomena. Considerable efforts are currently being undertaken to achieve clean experimental settings that show a minimal amount of noise and disorder and are close to zero temperature. A complementary direction investigates the interplay between coherent and dissipative processes. Recent experiments have revealed a glimpse into the emergence of a rich nonequilibrium behavior stemming from the competition of laser excitation, strong interactions, and radiative decay of Rydberg atoms. The aim of the present theoretical work is to show that local incoherent loss and gain of atoms can in fact be the source of interesting out-of-equilibrium dynamics. This perspective opens up paths for the exploration of nonequilibrium critical phenomena and, more generally, phase transitions, some of which so far have been rather difficult to study. To demonstrate the richness of the encountered dynamical behavior we consider here three examples. The first two feature local atom loss and gain together with an incoherent excitation of Rydberg states. In this setting either a continuous or a discontinuous phase transition emerges with the former being reminiscent of genuine nonequilibrium transitions of stochastic processes with multiple absorbing states. The third example considers the regime of coherent laser excitation. Here the many-body dynamics is dominated by an equilibrium transition of the “model A” universality class.

DOI: [10.1103/PhysRevA.93.023409](https://doi.org/10.1103/PhysRevA.93.023409)

I. INTRODUCTION

Identifying, classifying, and understanding the emergence of collective phenomena and other many-body effects is a central objective of physics. In the past decades the refinement of experimental techniques for preparing, addressing, and measuring atomic ensembles [1] opened entirely new possibilities for investigating not only stationary, but also dynamical properties of quantum many-body systems. Rich nonequilibrium physics often stems from the presence of competing dynamical processes and strong interactions. Amidst different platforms, gases of atoms excited to high-lying Rydberg states are currently receiving increasing attention [2–6] as they feature considerable interactions via dipole-dipole or van der Waals forces. Their interplay with the laser excitation process—inducing coherent Rabi oscillations on the atomic populations—has been shown to be the source of intricate behaviors, such as the formation of crystalline ground-state structures [7–9], collectively enhanced Rabi oscillations [10–12], or the emergence of correlated equilibrium states [13–17].

Since very recently, there has been considerable interest in understanding the many-body physics of interacting ensembles of Rydberg atoms in the presence of noise. While previously perceived as a detrimental feature, dissipation—caused by fluctuating atomic level shifts or radiative decay—can be in fact a source of an intriguingly rich dynamics. Examples include the occurrence of slow or glassy dynamics [18–21], the relaxation into stationary states with spatial correlations [22–24], the observation of intermittency and bistabilities [24–27], and the emergence of equilibrium [27–31] and out-of-equilibrium universal behavior [32].

In this work we introduce a scenario for the study of out-of-equilibrium phases and phase transitions with Rydberg atoms. The setting we have in mind consists of a background gas—acting as a large reservoir—from which Rydberg states

are only excited at given spatial positions which are arranged in a regular lattice, as produced, e.g., by employing spatial light modulators [33]. Atoms from the background dynamically enter and leave these excitation spots. In conjunction with the laser excitation and the strong interatomic interactions this local loss and gain dynamics leads to the emergence of nontrivial many-body dynamics. More specifically, as presented in Sec. III, in the presence of strong decoherence the loss and gain dynamics creates an absorbing space, rather than a single absorbing state. Remarkably, this leads to a partial loss of universality [34].

This scenario could be implemented in two rather different settings: in the first, a lattice of optical traps is immersed in a cold cloud of atoms and the traps are continuously filled and depleted [35]. Current experiments aim at progressively slowing down this local dynamics by, for example, reducing the pressure of the background gas or increasing the strength of the optical confinement [36–38]. These attempts could be reversed and, in principle, the setup could be “worsened” to the point that the time scale of the loss-and-gain dynamics becomes comparable with the other relevant dynamical processes. The second experimental setting consists of hot atomic gases confined in thermal vapor cells. Recently it has been shown that they indeed allow the observation of correlated many-body dynamics [20,27] when Rydberg states are excited. Our envisioned setup is then realized by restricting the laser excitation to a regular array of addressed spots. Thermal motion would move atoms in and out of these laser-illuminated regions, yielding the desired loss or gain dynamics.

Beyond introducing an additional dynamical process the consideration of local atom loss and gain might actually relax a number of challenges that are currently faced by experimentalists when studying collective many-body behavior in dissipative Rydberg lattices. It might also simplify the

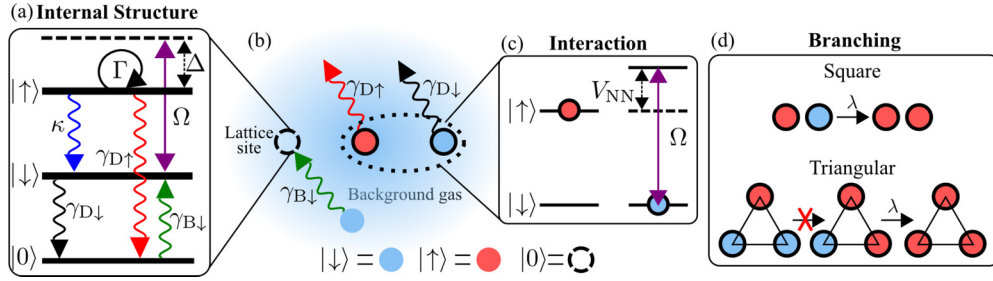


FIG. 1. Schematic representation of the system: (a),(b) an optical lattice is realized within a background cloud of atoms. Atoms within the sites undergo laser-induced coherent transitions between their ground state $|\downarrow\rangle$ and a high-lying (Rydberg) state $|\uparrow\rangle$. The corresponding Rabi frequency and laser detuning are Ω and Δ , respectively. A third state, $|0\rangle$, describes an empty or “inactive” site. Atoms are captured in and released from the sites with rates $\gamma_{B\downarrow}$ (capturing a ground-state atom), $\gamma_{D\downarrow}$ (losing a ground-state atom), and $\gamma_{D\uparrow}$ (losing an excited atom). The atomic states are furthermore subject to dephasing at a rate Γ . (c) Rydberg atoms interact with a van der Waals potential V_{kq} , whose value for nearest neighbors is denoted by V_{NN} . The corresponding energy shift of the Rydberg state in the vicinity of an excited atom is sketched. (d) Emergent branching processes in the limit of strong dephasing: in the case analyzed in Sec. III (square lattice) a single excitation has the potential for branching (with rate λ) which enables the production of larger clusters. In the case discussed in Sec. IV (triangular lattice) the system parameters are chosen such that two nearby excitations are required for a cluster to grow.

modeling of Rydberg gases in which typically radiative decay is accounted for as a dominant decoherence mechanism:

(i) It is not necessary to have (uniformly) deterministically loaded lattices, equal lattice confinement of ground state and Rydberg atoms, or very low-temperature states.

(ii) It is not necessary to construct lattice potentials that equally trap ground state and Rydberg atoms. In fact it is not necessary to keep atoms trapped over an entire experimental run.

(iii) One can employ very strongly interacting and high-lying Rydberg states that are typically long-lived. For such states the corresponding decay rate might simply be too small. In other words, it might be difficult to reach a regime in which the decay dynamics is able to properly compete with the laser excitation and interatomic interactions, which thus almost entirely characterize the evolution.

(iv) Even when acting on time scales that set it in competition with the driving, radiative decay is inevitably accompanied by momentum kicks from photon recoil. Even when a Rydberg atom eventually decays to the desired electronic ground the resultant heating might lead to loss of the atoms which can be accounted for in our description.

For the sake of simplicity and in order to focus on the behaviors introduced by the loss or gain dynamics we will not consider radiative decay processes in this work. The underlying assumption is that the loss or gain dynamics is faster than that of the decay and/or that decay effectively induces a loss process via the mechanism described in point (iv) above.

The paper is organized as follows: after defining the model in Sec. II we introduce two scenarios that respectively feature a continuous (Sec. III) and discontinuous (Sec. IV) dynamical phase transition to an effective absorbing subspace of states. Here we focus on a setting where the laser excitation of Rydberg states is described by a classical rate equation [39] due to the presence of strong dephasing noise. In Sec. V we discuss the case of a coherent laser in the framework of a mean-field approach. Here we show that the dynamics is described by the so-called “model A” universality class, similar to what has recently been found in dissipative Rydberg gases with radiative decay [28,29,31]. Concluding remarks are provided in Sec. VI.

II. MODEL

We employ the standard description of a Rydberg lattice gas where each atom is modeled in terms of an effective two-level system. The ground state $|\downarrow\rangle$ is coupled to a Rydberg nS state $|\uparrow\rangle$ through a laser with Rabi frequency Ω and a detuning Δ with respect to the atomic transition [see Fig. 1(a) for a visual representation]. Within the rotating wave approximation the many-body Hamiltonian is then given by

$$H = \Omega \sum_k \sigma_k^x + \Delta \sum_k n_k + \frac{1}{2} \sum_{k \neq p} V_{kp} n_k n_p, \quad (1)$$

where $V_{kp} = C_6/|\mathbf{r}_k - \mathbf{r}_p|^6$ represents the van der Waals (vdW) potential between pairs of excited atoms at positions \mathbf{r}_k and \mathbf{r}_p , and the sum runs over all lattice sites $k = 1 \dots L$. Interactions among ground-state atoms or between ground-state and Rydberg atoms are significantly weaker and will therefore be neglected. The operators $\sigma_k^{x/y/z}$ refer to the Pauli matrices in the $|\uparrow\rangle, |\downarrow\rangle$ subspace, i.e.,

$$\begin{aligned} \sigma_k^x &= |\uparrow_k\rangle\langle\downarrow_k| + |\downarrow_k\rangle\langle\uparrow_k|, \\ \sigma_k^y &= -i|\uparrow_k\rangle\langle\downarrow_k| + i|\downarrow_k\rangle\langle\uparrow_k|, \\ \sigma_k^z &= |\uparrow_k\rangle\langle\uparrow_k| - |\downarrow_k\rangle\langle\downarrow_k|. \end{aligned} \quad (2)$$

Furthermore, the local density of excitations is defined as $n_k = |\uparrow_k\rangle\langle\uparrow_k|$ and the density of ground-state atoms as $p_k = |\downarrow_k\rangle\langle\downarrow_k|$.

In order to account for atom gain or loss in the lattice sites we add an effective third state $|0\rangle$, denoting an empty (or “inactive”) site. We also introduce the corresponding local densities of active sites $e_k = n_k + p_k = |\uparrow_k\rangle\langle\uparrow_k| + |\downarrow_k\rangle\langle\downarrow_k|$. This local loss and gain takes place with atoms from a background gas which is assumed to act as a bath. In other words, the surrounding cloud contains a much higher number of atoms than can be accommodated in the lattice and the recapture of a lost one is an unlikely event. First of all, this suppresses correlations between loss and gain processes and allows us to treat them as being independent. Second, since atoms are constantly exchanged with new ones no correlations

can be produced in the system via these processes. Third, their occurrence probabilities are not appreciably affected by the history of occupation of a given site, and can thus be considered Markovian.

The relevant processes are schematically displayed in Fig. 1 and summarized below:

$$|\uparrow\rangle \xrightarrow{\gamma_{D\uparrow}} |0\rangle, \quad |\downarrow\rangle \xrightarrow{\gamma_{D\downarrow}} |0\rangle, \quad |0\rangle \xrightarrow{\gamma_{B\downarrow}} |\downarrow\rangle, \quad (3)$$

with $\gamma_{D\uparrow}$, $\gamma_{D\downarrow}$, and $\gamma_{B\downarrow}$ being the corresponding rates. The first two processes describe the loss of a Rydberg and ground-state atom, respectively. The third process corresponds to the capture of a ground-state atom from the background gas. Note that we do not consider the eventuality of Rydberg atoms being captured. The reason is that laser excitation to Rydberg states is restricted to local sites and consequently Rydberg atoms are not produced in the background gas. Hence, the transition $|0\rangle \rightarrow |\uparrow\rangle$ could only occur if a Rydberg atom is captured which had been previously expelled from another site, which is unlikely. Overall, this setting can also be described in terms of thermodynamic contact with baths at fixed chemical potentials, such that the ground-state atoms would be pushed to an equilibrium density $\gamma_{B\downarrow}/(\gamma_{B\downarrow} + \gamma_{D\downarrow})$, in contrast to the tendency towards depletion experienced by the excitations. Note that we are also neglecting processes which lead to the occupation of a given site with multiple atoms. In fact, in experiments with microtraps such multioccupancies are suppressed due to the collisional blockade [40,41]. In circumstances where such suppression is not taking place the so-called dipole or Rydberg blockade [38,42,43] is ensuring that each site can only feature a single Rydberg excitation. This also limits the local site dynamics to a restricted space at the expense of a possibly varying local (density-dependent) Rabi frequency [44]. For the sake of simplicity we will not consider such situations in this work.

In addition to the loss or gain dynamics we consider the presence of noise, which dephases local superpositions between the states $|\uparrow\rangle$ and $|\downarrow\rangle$ at a rate Γ . The origin of this noise can be fluctuating background fields that result in random atomic level shifts, the broadening of atomic lines due to Doppler [20] or interaction effects [45], or a spectrally broad excitation laser [2].

In the presence of the described coherent and dissipative processes the evolution of the density matrix ρ of the system is governed by a quantum master equation in Lindblad form [46,47],

$$\begin{aligned} \partial_t \rho = & -i[H, \rho] + \sum_{i,k} \gamma_i \left[L_{i,k} \rho L_{i,k}^\dagger - \frac{1}{2} \{L_{i,k}^\dagger L_{i,k}, \rho\} \right] \\ & + \sum_k \Gamma \left[n_k \rho n_k - \frac{1}{2} \{n_k, \rho\} \right]. \end{aligned} \quad (4)$$

Here the index i runs over the three different sources of noise introduced in Eq. (3), while k over all lattice sites and $\{A, B\} = AB + BA$, is shorthand for an anticommutator. $L_{D\downarrow,k} = |0_k\rangle\langle\downarrow_k|$, $L_{D\uparrow,k} = |0_k\rangle\langle\uparrow_k|$, and $L_{B\downarrow,k} = |\downarrow_k\rangle\langle 0_k|$ are the corresponding local jump operators; the last term accounts for dephasing, implemented via the jump operators n_k .

III. CONTINUOUS TRANSITION FROM/TO AN ABSORBING STATE

We start by considering a situation in which the dephasing amplitude Γ is much larger than the Rabi frequency and the other dissipative rates ($\Gamma \gg \Omega, \gamma_i$). In this regime, the dynamics is effectively described by means of a classical stochastic equation [18,39,48,49]: the underlying separation of time scales permits the adiabatic elimination of the portion of the phase space subject to dephasing. Correspondingly, the evolution of the density matrix ρ of the system is projected onto the dissipation-free subspace [50–52], which in this case corresponds to the sole diagonal components in the σ^z basis (i.e., a basis of classical spin configurations) [39]. At the leading order in a perturbative expansion in powers of γ_i/Γ and Ω/Γ the truncated density matrix μ evolves according to

$$\begin{aligned} \partial_t \mu = & \sum_k \Lambda_k (\sigma_k^x \mu \sigma_k^x - e_k \mu) \\ & + \sum_{i,k} \gamma_i \left[L_{i,k} \rho L_{i,k}^\dagger - \frac{1}{2} \{L_{i,k}^\dagger L_{i,k}, \rho\} \right], \end{aligned} \quad (5)$$

where

$$\Lambda_k = \Omega^2 \Gamma \left[\left(\frac{\Gamma}{2} \right)^2 + \left(\Delta + \sum_{q \neq k} V_{kq} n_q \right)^2 \right]^{-1} \quad (6)$$

is a configuration-dependent rate. We emphasize here that this effective dynamics takes place within the subspace of classical configurations, therefore, it is entirely determined by loss or gain processes and the laser driving, while the dephasing—by construction—plays no role at this level. This corresponds to the fact that there is no 0th-order term in the perturbative expansion above, i.e., for $\Omega = \gamma_i = 0$ the effective dynamics is completely trivial.

Defining the diagonal part of the Hamiltonian ($H|_{\Omega=0}$) as the “classical” component, the second term in the brackets of Eq. (6) corresponds to the square of the classical energy change accompanying a spin flip at site k . Spin flips that result in a significant increase or decrease in energy are therefore strongly suppressed. In the scenario investigated in this section we choose the detuning Δ such that it is opposite to the interaction energy V_{NN} between neighboring excited atoms ($\Delta = -V_{NN}$) [see Fig. 1(c)]. Hence, exciting an atom right next to an *isolated* already excited one incurs no energy difference and therefore occurs at the maximal rate $\Lambda_k^{(\max)} \equiv \lambda = 4\Omega^2/\Gamma$ [see Fig. 1(d)]. We further assume to be working in a regime where $-\Delta = V_{NN} \gg \Gamma$, i.e., the interaction surpasses the dephasing strength. In this regime any atom that has more than 1 excitation in its neighborhood (or none at all), can only change its internal state at a rate of order $\Lambda_k \propto \Omega^2 \Gamma / \Delta^2$. This rate is significantly smaller than $\Lambda_k^{(\max)}$ and thus such processes are strongly suppressed. For brevity, we shall refer to all of them as “off-resonant” processes. Among them, we emphasize that the creation of excitations in an empty neighborhood, occurring at a rate $\Lambda_k \approx \Omega^2 \Gamma / \Delta^2$, is also strongly suppressed.

In order to gain some insight into the expected many-body dynamics we assume for a moment that all off-resonant processes can be neglected. In this regime Eqs. (5) and (6) display

features that characterize a class of stochastic processes [34], such as the contact process and other branching-annihilating ones, which are known to undergo genuine nonequilibrium phase transitions [53,54]. By this, we mean that these system have no equilibrium counterpart whatsoever within their universality class; for instance, there is no thermal system which displays the same scaling behaviors. This is due to the breaking of a subtle symmetry, generally referred to as *microreversibility* [55–58], which for stochastic processes corresponds to detailed balance [59]. Proper nonequilibrium criticality thus emerges when this symmetry is not present nor recovered upon rescaling, i.e., if the out-of-equilibrium perturbation is not irrelevant in the renormalization-group sense.

The branching-annihilating processes mentioned above feature an absorbing phase with strictly zero density $n = \sum_k \langle n_k \rangle / L$, i.e., in the absence of excitations no new ones can be created. Furthermore, the production of excitations can only proceed via nucleation of clusters and is, in this sense, local (it cannot occur arbitrarily far from pre-existing excitations). It is important to note that in the present case the absorbing phase does not consist of a unique state, but rather an absorbing space that is spanned by the entire set of configurations of sites which are either in state 0 or state \downarrow . In general there is dynamics taking place within the absorbing manifold as all the absorbing configurations can be visited via the interplay of the local loss and gain processes with rates $\gamma_{D\downarrow}$ and $\gamma_{B\downarrow}$. This requires us to consider also the density of active sites $\eta = \sum_k \langle e_k \rangle / L$ when analyzing the dynamics of the system.

A. Mean-field approach

The mean-field approximation discards correlations between different sites—i.e., for every local observable \mathcal{O}_k we substitute $\langle \mathcal{O}_k \mathcal{O}_p \rangle \rightarrow \langle \mathcal{O}_k \rangle \langle \mathcal{O}_p \rangle$ if $k \neq p$ —and permits the formulation of closed equations of motion for the expectation values of the densities of excitations n and of active sites η :

$$\partial_t n = -\gamma_{D\uparrow} n + \sum_{j=0}^z \binom{z}{j} \lambda_j n^j (\eta - 2n)(1-n)^{z-j}, \quad (7a)$$

$$\partial_t \eta = \gamma_{B\downarrow} - (\gamma_{B\downarrow} + \gamma_{D\downarrow}) \eta + (\gamma_{D\downarrow} - \gamma_{D\uparrow}) n. \quad (7b)$$

Here, z is the lattice coordination number (number of nearest neighbors per site) and λ_j is shorthand for the rate of a flipping process occurring in the presence of j excited neighbors. This means that λ_1 characterizes the resonant processes introduced above (and $\lambda_1 = \lambda = 4\Omega^2/\Gamma$), whereas the remaining values refer to the off-resonant processes and read

$$\lambda_{j \neq 1} = \frac{\Omega^2 \Gamma}{\left(\frac{\Gamma}{2}\right)^2 + \Delta^2(j-1)^2} \approx \frac{\Omega^2 \Gamma}{\Delta^2(j-1)^2} \ll \lambda. \quad (8)$$

In a first approximation we neglect them altogether and Eq. (7a) becomes

$$\partial_t n = -\gamma_{D\uparrow} n + \lambda z n (\eta - 2n)(1-n)^{z-1}. \quad (9)$$

This equation together with Eq. (7b) predicts a transition from the region $\lambda < \lambda_c = \gamma_{D\uparrow}(\gamma_{B\downarrow} + \gamma_{D\downarrow}) / (z\gamma_{B\downarrow})$ which admits only the absorbing solution $n = 0$ to the region $\lambda > \lambda_c$ in which the system displays a finite density $n > 0$ in the long-time limit. In Fig. 2 we report the corresponding phase

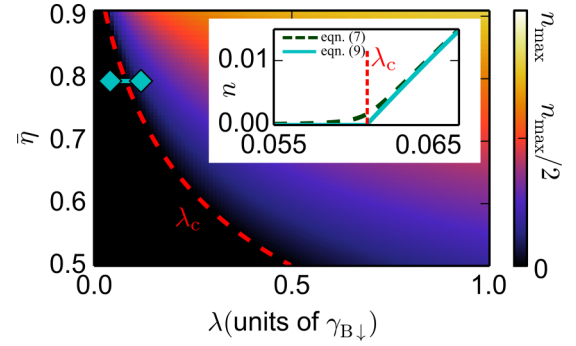


FIG. 2. Stationary density of excitations n extracted from the mean-field equations (9) and (7b) for $-\Delta = V_{NN} = 64\Gamma$, $\gamma_{B\downarrow} = 0.01\Gamma$, and $\gamma_{D\uparrow} = \gamma_{D\downarrow}$. The data are shown as a function of the branching rate λ for resonant processes and the density of active sites $\eta = \gamma_{B\downarrow} / (\gamma_{B\downarrow} + \gamma_{D\downarrow})$. The color scale is bounded by $n_{\max} = 0.5$. The red dashed line corresponds to the values taken by the critical rate λ_c for different values of η . A cross section is displayed in the inset for $\eta = 0.8$ (along the cyan horizontal line in the main figure), which highlights the mean-field scaling behavior $n \sim \lambda - \lambda_c$. The green, dashed line corresponds to the same curve calculated including the leading off-resonant processes relevant in a Rydberg gas. As expected, the introduction of the latter makes the transition smoother, but deviations are only visible in close vicinity to the critical point λ_c .

diagram for the choice $\Delta = -64\Gamma$, $\gamma_{D\uparrow} = \gamma_{D\downarrow} \equiv \gamma_D$ in the $\lambda - \eta$ plane, where the symbol η denotes the stationary density of active sites. The threshold value λ_c identifies the critical point of a continuous transition between the two phases. To its right, the density scales linearly ($n \sim \lambda - \lambda_c$), while at the critical point its value decays to 0 in time according to the power law $n(t) \sim 1/t$. The density of active sites relaxes to the finite value $\gamma_{B\downarrow} / (\gamma_{B\downarrow} + \gamma_{D\downarrow})$. Consequently, at the mean-field level, this system undergoes a transition which shows some of the characteristic features of directed-percolation (DP) universality [34].

Let us now discuss the role of the off-resonant terms. Those with $j > 1$ in Eq. (7a) do not affect the fundamental properties of the transition, as they vanish for $n \rightarrow 0$. Therefore, they can only shift the position of the critical point according to the relative statistical weights λ_j . The $j = 0$ term, on the other hand, constitutes a relevant—albeit small—perturbation that brings the system away from the critical point. The reason is that it accounts for production of excitations in an empty neighborhood and thus prevents the aforementioned subspace of configurations devoid of excitations from being strictly absorbing. This term smooths the transition into a crossover, as highlighted in the inset of Fig. 2. The magnitude of this effect can be suppressed by increasing the detuning Δ . When sufficiently small it allows the observation of the mean-field scaling behavior for values of $\lambda \gtrsim \lambda_c$.

B. Numerical analysis

In order to investigate the effect of fluctuations which are not captured by the mean-field treatment we perform numerical Monte Carlo simulations, using a state in which all sites are occupied with a Rydberg atom as the initial condition. We set the rates $\gamma_{D\downarrow} = \gamma_{D\uparrow} \equiv \gamma_D$, $\gamma_{B\downarrow} = 0.01\Gamma$, $V_{NN} = 64\Gamma = -\Delta$ and collect data for several values of the

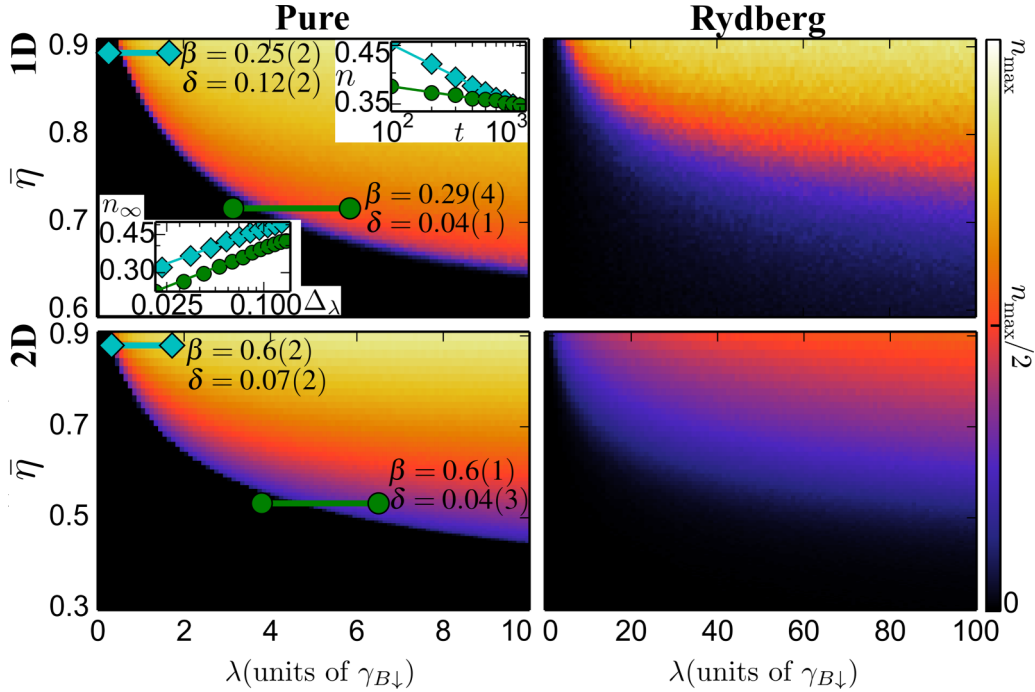


FIG. 3. Phase diagrams of the pure and the Rydberg process (see text) in the $\bar{\eta}$ - λ plane for a 1D chain of 100 sites and a 2D square lattice of 20×20 sites. The parameters are chosen as $-\Delta = V_{\text{NN}} = 64\Gamma$, $\gamma_{B\downarrow} = 0.01\Gamma$, and $\gamma_{D\downarrow} = \gamma_{D\uparrow} \equiv \gamma_D$. The color scale is set with respect to the maximal value the density can take, i.e., $n_{\text{max}} = 1$ for the pure process and $1/2$ for the Rydberg one. Numerically computed exponents β (static) and δ (dynamic) are displayed in the panels. The selected parameter ranges are shown as a cyan and a green line on the main plot. For the 1D pure process we also show (in log-log scale) the critical profiles of the stationary density n as a function of $\Delta\lambda = \lambda - \lambda_c$ (lower-left inset) and of its evolution in time (upper-right inset) to highlight the scaling behavior. For comparison we provide the known DP exponents [34]: $\beta_{1\text{D}} = 0.276$, $\beta_{2\text{D}} = 0.584$, $\delta_{1\text{D}} = 0.159$, and $\delta_{2\text{D}} = 0.451$.

parameters γ_D and Ω . For this particular choice of parameters the loss and gain dynamics decouples from the excitation dynamics. This can be seen directly in Eq. (7b) which is valid beyond mean field. Consequently, the density of active sites η reaches exponentially fast [on a time scale $(\gamma_{B\downarrow} + \gamma_D)^{-1}$] the steady-state value $\bar{\eta} = \gamma_{B\downarrow}/(\gamma_{B\downarrow} + \gamma_D)$.

For Rydberg gases one needs to account for the fact that the off-resonant production of excitations and the long-range tails of the vdW potential affect the emergence of the phase transition. As we discuss further below, these features actually constitute a source of additional noise which to some extent may obscure the anticipated scaling behaviors. In order to shed light on the fundamental critical properties of the transition we have therefore also simulated a dynamical process in which we replace the first term of the right-hand side of Eq. (5) by

$$\sum_{k,i \in \{k\}} \frac{\lambda}{2d} n_i (\sigma_k^+ \mu \sigma_k^- - p_k \mu), \quad (10)$$

with $\{k\}$ denoting the set of nearest-neighboring sites of site k and d being the dimension. After this replacement we have a pure branching process (as found, e.g., in the contact process mentioned above [34]) producing excitations from nearby ones at a rate $\lambda/(2d)$. The normalization by the quantity $2d$ —which corresponds to z for square lattices—is meant to compensate for the fact that in this case multiple excitations enhance the rate. We emphasize that, although different, the two

processes we consider share the same fundamental properties: the absorbing subspace is the same and, apart from off-resonant events, branching is the only way to increase the number of excitations. Furthermore, in the presence of low densities—as happens in the proximity of the critical point—the action of the branching terms in Eqs. (5) and (10) is analogous up to multiplicative factors. For brevity, in the following we shall refer to the new stochastic process as the “pure” instance and to the original process [Eq. (5)] as the “Rydberg” one.

In Fig. 3 we show the stationary value (obtained from Monte Carlo simulations) of the density of excitations n in the $\bar{\eta}$ - λ plane for one-dimensional (1D) (100 sites) and 2D (20×20 sites) square lattices in both cases. The pure and the Rydberg processes display qualitatively the same behavior. As expected, in the pure case the transition from the absorbing to the active phase is significantly sharper. Beyond that, two interesting features can be observed. First, the simulations seem to suggest that the critical point λ_c diverges as the stationary density of active sites $\bar{\eta}$ decreases and that below a certain threshold $\bar{\eta}_c$ the transition disappears entirely. Second, there is a qualitative difference in the static and dynamic scaling behavior when varying $\bar{\eta}$. The stationary properties remain unaffected and always display, within numerical accuracy, a scaling behavior $n \sim (\lambda - \lambda_c)^\beta$ with a critical exponent β compatible with the DP one for both one- and two-dimensional processes (see Fig. 3). In contrast, the dynamical approach to stationarity changes continuously. This means that when approaching the

threshold value $\bar{\eta}_c$, the critical exponent of the algebraic decay $n(t) \sim t^{-\delta}$ smoothly decreases to 0 from a value which, in one dimension, is comparable with the one of pure DP. We have verified in one dimension that this behavior is only weakly affected by finite-size effects conducting simulations on lattices with 1000 and 10 000 sites.

The presence of a varying exponent is strongly reminiscent of the behavior of stochastic processes with multiple absorbing states as reported in Refs. [34,60], which provide a qualitative explanation of our observations. Even though in our case the absorbing space is not made of individually absorbing states, the excitation dynamics effectively perceives them as such, since it stops completely as soon as the first absorbing configuration is reached. In other words, once the evolution ends within this subspace the excitation density—our order parameter—remains at 0. Moreover, in the cases discussed in Refs. [34,60] the dynamic exponent is also not constant but instead varies continuously as a function of the initial conditions, e.g., the initial density. This relates to the fact that the initial condition can ultimately determine the properties of the absorbing state one ends up with. The initial condition thus seems to act as a purely marginal parameter under renormalization-group flows [61]; consequently, fixing the dynamical rates at criticality and tuning its value implies moving along a line of critical points with continuously varying exponents, which matches the numerical observations. Furthermore, not all the properties of the initial state survive coarse graining: for example, if the density does not rescale and remains unmodified, the initial correlation length progressively shrinks towards 0, implying that the order parameter density is the only “relevant” property to account for, as highlighted in Ref. [60]. Analogous features have been identified in non-Markovian systems [34]. Moreover, in Ref. [62] it is argued that in many models with multiple absorbing states the emerging nonuniversal features are due to an effective memory encoded in the dynamics.

In our simulations we start from a fixed initial condition (all atoms present and excited). However, the fast loss or gain dynamics rapidly constructs an “effective initial condition” with an active site density $\bar{\eta}$ determined by the rates $\gamma_{B,\downarrow}$ and γ_D . On average, the value of $\bar{\eta}$ remains subsequently constant in the evolution and thus characterizes the properties of the stationary state as well. Following the same reasoning applied to the idealized models mentioned above, if we imagine $\bar{\eta}$ to be a marginal parameter which does not flow under renormalization-group transformations, we can relate the continuous variation of the dynamical exponents we observe to the same underlying structure, i.e., to the movement along a line of critical points in a marginal direction.

The Rydberg case features off-resonant processes and thus displays a smoothed transition, as shown in the right-hand column of Fig. 3: more specifically, as mentioned above, there is a small, but finite probability of exciting ground-state atoms even far away from any excitation; as a consequence, the absorbing property of the pure case is broken and there can be rare jumps outside of the (quasi)absorbing subspace. This constitutes a relevant perturbation out of the critical region and implies the impossibility of observing a sharp transition. The low amplitude of these terms, however, makes the two distinct phases still emerge, as can be seen in the right-hand panels.

Second, it requires stronger driving for the active phase to appear. This can be understood by noting how clusters of excitations actually hinder their own growth. For instance, if we consider a pair of nearby excitations, elongating it to a three-excitation segment ($\uparrow\uparrow\downarrow \rightarrow \uparrow\uparrow\uparrow$) faces the presence of next-nearest-neighbor interactions. Because of them, the rate at which this process occurs is no longer λ but instead given by

$$\Lambda_k^{(\text{NNN})} = \frac{\Omega^2 \Gamma}{\left(\frac{\Gamma}{2}\right)^2 + V_{\text{NNN}}^2}. \quad (11)$$

Our choice of parameters, $V_{\text{NNN}} = V_{\text{NN}}/2^6 = \Gamma$, implies $\Lambda_k^{\text{NNN}} = \lambda/5$ and hence the branching rate is effectively reduced. Further growth along the same direction experiences much smaller corrections and thus continues approximately at a rate $\lambda/5$. The situation worsens if we consider branching orthogonally with respect to the two original excitations, since in this case the distance between next-nearest neighbors is reduced to $\sqrt{2}$ times the lattice spacing, implying $V_{\text{NNN}} = V_{\text{NN}}/(\sqrt{2})^6 = 8\Gamma$ and yielding an effective rate $\Lambda_k^{\text{NNN}} = \lambda/257$. This explains the suppression of the stationary density in the 2D case with respect to the 1D one. The relevance of this effect can be drastically reduced by partially removing the tails of the vdW interactions using a microwave dressing scheme (see Refs. [32,63–65]). In other words, by coupling two Rydberg levels with a strong microwave field one can obtain a hybridization of the relative interactions. For appropriate choices, the latter features a crossover threshold separating a short-distance regime displaying the usual vdW decay from a long-distance one which is instead suppressed with respect to the previous one and can be considered approximately flat. This length scale thus acts as a cutoff for the potential tails.

IV. DISCONTINUOUS ABSORBING-STATE PHASE TRANSITION

The continuous phase transition discussed above is not merely due to the competition between system-filling and system-emptying processes. It also strongly relies on the resonance condition requiring the presence of a single excitation nearby, which constitutes a fundamental connection with other classical branching processes [34].

To demonstrate this we consider a 2D triangular lattice ($z = 6$) of Rydberg atoms which is irradiated by a laser with detuning $-\Delta = 2V_{\text{NN}}$. This implies that atoms now require exactly two excited neighbors to be effectively brought in resonance with the laser [see Fig. 1(d)]. With this constraint, the geometrical structure of the lattice becomes relevant: for instance, clusters cannot grow on a square lattice, since neighboring sites do not share common neighbors.

A. Mean-field approach

The density of active sites is evolving according to Eq. (7b) in this case as well. The evolution equation for the excitation density n can be cast in the form (7a), but with λ_j redefined as $\lambda_2 = \lambda$ and

$$\lambda_{j \neq 2} = \frac{\Omega^2 \Gamma}{\left(\frac{\Gamma}{2}\right)^2 + \Delta^2(j-2)^2} \approx \frac{\Omega^2 \Gamma}{\Delta^2(j-2)^2} \ll \lambda. \quad (12)$$

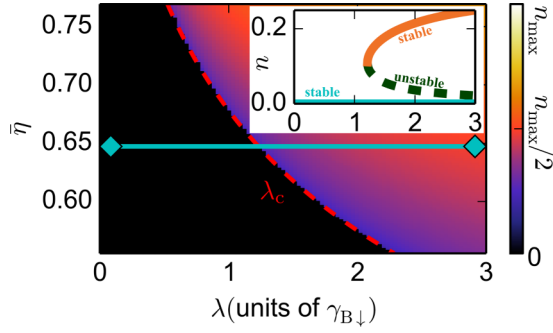


FIG. 4. Stationary density of excitations n (we select the stable solution with highest value) extracted from the mean-field equations (13) and (7b). The data are shown as a function of λ (branching rate) and $\bar{\eta}$ (stationary density of active sites) for $-\Delta = 2V_{\text{NN}} = 64\Gamma$, $\gamma_{B\downarrow} = 0.01\Gamma$, and $\gamma_{D\uparrow} = \gamma_{D\downarrow}$. Here $n_{\text{max}} = 0.5$. The dashed line corresponds to the critical rate λ_c for different values of $\bar{\eta}$. In the inset we plot the profiles of the three stationary solutions of Eq. (13) for $\bar{\eta} \approx 0.65$ in a parameter interval indicated by the cyan horizontal line in the main figure. The absorbing solution is displayed as a solid, cyan line which never leaves 0. The upper solid orange line represents the stable solution with finite density which only occurs for $\lambda > \lambda_c$. The dashed green line corresponds to the third, unstable solution.

Hence, the dominant contribution is now given by the $j = 2$ term, i.e.,

$$\partial_t n \approx -\gamma_{D\uparrow} n + \frac{2z(z-1)\Omega^2}{\Gamma} n^2(\eta - 2n)(1-n)^{z-2}. \quad (13)$$

Introducing the parameter $\chi = 2z(z-1)\Omega^2/\Gamma\gamma_{D\uparrow} = \lambda z(z-1)/2\gamma_{D\uparrow}$, these mean-field equations predict a discontinuous transition from a phase $\chi < \chi_c$ in which the only acceptable stationary solution is $n = 0$ to an active phase ($\chi > \chi_c$) in which two further solutions appear (constituting a *saddle-node bifurcation* [66]; see inset of Fig. 4). These correspond to additional real roots of the right-hand side of Eq. (13) and are identified by the equality $\chi n(\bar{\eta} - 2n) = (1-n)^{2-z}$. Thus, the threshold value for χ corresponds to

$$\chi_c = \min_{n \in [0, 1/2]} \frac{1}{n(\bar{\eta} - 2n)(1-n)^{z-2}}. \quad (14)$$

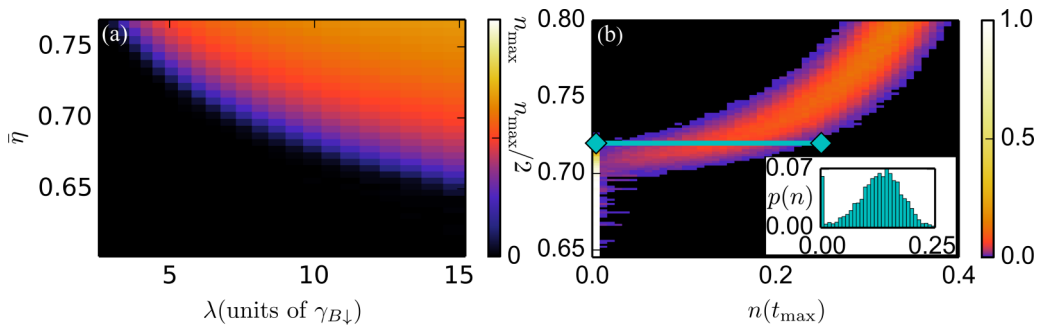


FIG. 5. (a) Stationary density profile in the λ - $\bar{\eta}$ plane for the branching process defined on a 25×25 triangular lattice. The color scale extends up to $n_{\text{max}} = 0.5$. As in the mean-field treatment in Fig. 4, we fix $-\Delta = 2V_{\text{NN}} = 64\Gamma$, $\gamma_{B\downarrow} = 0.01\Gamma$, and $\gamma_{D\uparrow} = \gamma_{D\downarrow} \equiv \gamma_D$. For a sufficiently large population of trapped atoms (sufficiently small loss rate γ_D) and large enough λ ($\propto \Omega^2$), the process becomes clearly capable of maintaining a finite density of excitations for long times. (b) Counting statistics $p(n)$ of the final density $n(t_{\text{max}})$ at fixed $\Omega = 0.125\Gamma$ and $\Gamma t_{\text{max}} = 25000$ as a function of $\bar{\eta}$. Bimodality is a signature of the discontinuity of the phase transition and becomes clearly visible in the inset section taken along a section at $\bar{\eta} \approx 0.7194$.

Branching off from a common point [the value n yielding the minimum in Eq. (14)], one of these solutions is unstable (dashed green line in the inset of Fig. 4) under small perturbations and decreases asymptotically to 0, whereas the other one (solid blue line) is stable and increases up to $\bar{\eta}/2$. The absorbing solution remains always stable. A phase diagram for this case is shown in the main panel of Fig. 4, where we display, for various choices of λ and $\bar{\eta}$, the largest stable mean-field solution, in order to highlight the finite jump experienced by this value when the boundary $\lambda_c = 2\gamma_{D\uparrow} \chi_c/[z(z-1)]$ is crossed. The quantitative effect of the off-resonant terms is again barely noticeable at the mean-field level and we thus do not display it. We recall, however, that the subspace of configurations with $n = 0$ is not perfectly absorbing and thus the lower branch is slightly lifted from 0.

B. Numerical analysis

To study the system beyond mean field we employ Monte Carlo simulations. The parameters are identical to the previous simulations with the exception that $V_{\text{NN}} = -\Delta/2 = 32\Gamma$. Again, we set $\gamma_{D\downarrow} = \gamma_{D\uparrow} \equiv \gamma_D$ and use a completely filled initial state from which the fast site dynamics will generate an effectively random initial configuration. In Fig. 5 we display the stationary density n in the Ω - γ_D plane. Note that for the sake of clarity we do not include interactions beyond nearest neighbors, i.e., we assume that the tails of the vdW potential are modified for example by the previously mentioned microwave dressing [32,63–65]. Their inclusion does not qualitatively change the phase diagram, although it makes it more difficult to highlight the discontinuous nature of the transition. As predicted by the mean-field study we observe the presence of both an absorbing phase and an active one. At a first glance the data suggest the presence of a continuous crossover instead of a discontinuous jump. This can be reconciled with the previous Subsection's conclusions by considering that in the presence of two stable stationary solutions, different realizations of the stochastic process end up in either one or the other. However, this information is lost once the average is taken.

We have therefore computed the counting statistics—or probability distribution—of the excitation density n at the maximal time of our simulations, $\Gamma t_{\text{max}} = 15000$. It is displayed in Fig. 5(b) and clearly highlights the discontinuous

first-order nature of the transition showing that indeed, for a certain range of parameters, the distribution becomes bimodal. This confirms that some initial conditions decay into empty configurations, whereas other ones maintain a finite density $n > 0$ for long times.

V. MODEL A UNIVERSALITY

For completeness we now briefly discuss the situation in which dephasing is not strong enough in order to warrant a description of the dynamics of the system in terms of effectively classical evolution equations. In this situation the full quantum master equation (4) needs to be solved which can be done numerically only for systems consisting of a few sites. To nevertheless gain a qualitative understanding of the emerging phase structure we employ a mean-field treatment. The single-site expectation values $\langle n_k \rangle = n$, $\langle p_k \rangle = p$, $\langle \sigma_k^x \rangle = S^x$ and $\langle \sigma_k^y \rangle = S^y$ evolve according to equations

$$\dot{n} = \Omega S^y - \gamma_{D\uparrow} n, \quad (15a)$$

$$\dot{p} = -\Omega S^y - \gamma_{D\downarrow} p + \gamma_{B\downarrow} (1 - n - p), \quad (15b)$$

$$\dot{S}^x = -(\Delta + Vn)S^y - \frac{\Gamma + \gamma_{D\uparrow} + \gamma_{D\downarrow}}{2} S^x, \quad (15c)$$

$$\dot{S}^y = 2\Omega(p - n) + (\Delta + Vn)S^x - \frac{\Gamma + \gamma_{D\uparrow} + \gamma_{D\downarrow}}{2} S^y, \quad (15d)$$

where $V = \sum_q V_{kq}(1 - \delta_{kq})$.

First, we focus on investigating the stationary properties. Setting the time derivatives to zero one can relate all steady-state expectation values to the excitation density n , i.e.,

$$S^y = \frac{\gamma_{D\uparrow}}{\Omega} n, \quad (16a)$$

$$p = \frac{-\gamma_{D\uparrow} n + \gamma_{B\downarrow} (1 - n)}{\gamma_{B\downarrow} + \gamma_{D\downarrow}}, \quad (16b)$$

$$S^x = -2 \frac{\Delta + Vn}{\Gamma + \gamma_{D\uparrow} + \gamma_{D\downarrow}} \frac{\gamma_{D\uparrow}}{\Omega} n. \quad (16c)$$

This leads to a closed polynomial equation for the excitation density in the stationary state which reads

$$n[a + b(c + n)^2] = 1, \quad (17)$$

where we have introduced the parameters

$$a = \frac{2\gamma_{B\downarrow} + \gamma_{D\uparrow} + \gamma_{D\downarrow}}{\gamma_{B\downarrow}} + \frac{(\Gamma + \gamma_{D\uparrow} + \gamma_{D\downarrow})\gamma_{D\uparrow}(\gamma_{B\downarrow} + \gamma_{D\downarrow})}{4\Omega^2\gamma_{B\downarrow}},$$

$$b = \left(\frac{V}{\Omega}\right)^2 \frac{\gamma_{D\uparrow}(\gamma_{B\downarrow} + \gamma_{D\downarrow})}{\gamma_{B\downarrow}(\Gamma + \gamma_{D\uparrow} + \gamma_{D\downarrow})}, \quad \text{and} \quad c = \frac{\Delta}{V}. \quad (18)$$

Similar mean-field equations have been obtained in a number of recent works [24,27,28,67,68] which investigate the dynamics of Rydberg gases in the presence of radiative decay. A known feature of Eq. (17) is that it describes a bistable behavior, not fundamentally different from the one encountered in the previous section, i.e., for certain values of the physical parameters the mean-field equations of motion admit two, instead of one, stable stationary solutions.

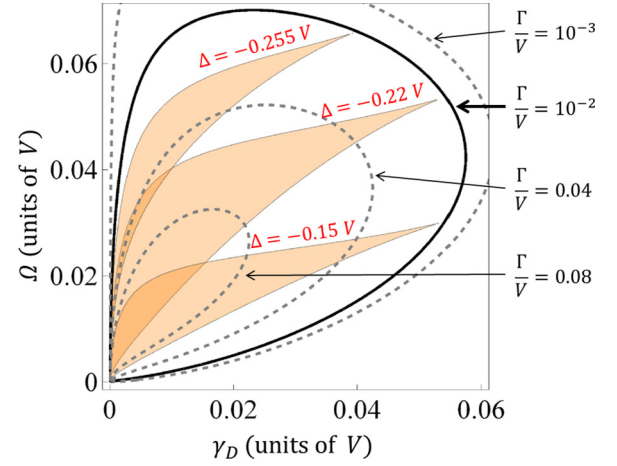


FIG. 6. Stationary phase diagram of the mean-field equations of motion (15a)–(15d) for three different detunings Δ in the plane spanned by Ω/V and $\gamma_{D\downarrow}/V = \gamma_{D\uparrow}/V \equiv \gamma_D/V$. The shaded areas correspond to the bistable regions for $\Gamma = 0.01V$ and $\gamma_{B\downarrow} = \gamma_D$. Points lying outside represent choices for which there is only one physical solution. From top to bottom, the detuning is fixed at $-0.255V$, $-0.22V$, and $-0.15V$. The boundaries of each shaded region meet with vanishing net angle at the corresponding critical point (red disk). The solid black line displays the path taken by the critical point as Δ is varied. The dashed lines show how the profile of this path shrinks when the dephasing rate Γ is increased. From the outermost to the innermost, the values correspond to $\Gamma = 0.001V$, $0.01V$ (solid line), $0.04V$, and $0.08V$. The transition disappears when $\Gamma/V \geq \gamma_{B\downarrow}/4(\gamma_{B\downarrow} + \gamma_D) = 0.125$. The bistable region is also absent when Δ/V lies outside the interval $[-9\gamma_{B\downarrow}/[16(\gamma_{B\downarrow} + \gamma_D)], 0] = [-9/32, 0]$.

Figure 6 provides a representative example of the phase diagram's structure in the $\gamma_D - \Omega$ plane, obtained in the plot for the specific choice $\gamma_{D\uparrow} = \gamma_{D\downarrow} = \gamma_{B\downarrow} = \gamma_D$. The bistable regions are shown as shaded areas. In general, the lines delimiting these domains meet with vanishing angle in a critical point (see also the discussion in Ref. [28]) which for fixed parameter c is located at $a_c = -9/8c$, $b_c = -27/8c^3$. This identifies a unique direction, which in the parameter space spanned by a , b , and c reads $\delta a = -\delta b c^2/9$ where $\delta a = a - a_c$ and $\delta b = b - b_c$. Varying the parameters in such a way to follow this path, the profile of the stationary density displays a branching at the critical point which can be related to the spontaneous breaking of a \mathbb{Z}_2 symmetry [28]. The solutions for the stationary density of excitations take here the form $n = n_c + \delta n$, with the critical density $n_c = -2c/3$ and

$$\delta n = \begin{cases} 0 & (\delta b < 0), \\ \pm \frac{2c}{3} \sqrt{\frac{\delta b}{\delta b + b_c}} \sim \pm \delta b^{1/2} & (\delta b > 0). \end{cases} \quad (19)$$

Crossing the critical point along any other direction yields instead a behavior $\delta n \sim \delta b^{1/3}$, which relates to an explicit breaking of the symmetry. This is identical to the situation that is encountered in the thermodynamics of a ferromagnet in the presence of a finite magnetic field.

To understand the dynamical behavior near the critical point we first note that for our choice of parameters $\gamma_{D\downarrow} = \gamma_{D\uparrow} = \gamma_D$

the site dynamics decouples. The corresponding equation is

$$\partial_t(n + p) = \dot{\eta} = \gamma_{B\downarrow} - (\gamma_{B\downarrow} + \gamma_D)\eta. \quad (20)$$

Linearizing the remaining equations in the proximity of the critical point, we find two attractive modes and a vanishing one, signaling the presence of a critical slowing down of the dynamics, i.e., an algebraic relaxation towards the stationary value $n(t) - n_c \sim t^{-1}$.

Recent experiments in Rydberg gases suggest that a mean-field treatment such as the one presented here can correctly capture qualitative dynamical and static features [27,31]. A recently developed variational method [29,30], which improves on the mean field, showed in this context that the bistable region is in fact “replaced” by a first-order-transition line terminating in a critical point. The latter is related to an emerging universality belonging to the so-called model A (or Ising-Glauber) class [69]. The lines separating the bistable and stable regions can consequently be interpreted as spinodal lines, resulting in the appearance of long-lived metastable states which have been observed experimentally [27] and whose properties relate to the mean-field predictions [28].

Hence, the results in this section indicate that the interplay between the coherent laser excitation, the interaction and the loss or gain dynamics can drive the system towards a classical equilibrium critical point. Finally, we remark that here—contrary to the cases presented in Secs. III and IV—the presence of dephasing is inessential for the emergence of criticality. Moreover, the transition disappears when the dephasing rate exceeds

$$\Gamma_c = \frac{1}{2} \frac{\gamma_{B\downarrow}}{2\gamma_{B\downarrow} + \gamma_{D\downarrow} + \gamma_{D\uparrow}} V - \gamma_{D\uparrow} - \gamma_{D\downarrow}$$

as indicated in Fig. 6. From a physical point of view, this can be understood by the fact that the various cases reported here rely on facilitation effects induced by the blue detuning of the laser with respect to the atomic transition. As discussed above, this means that the presence of excited atoms enhances the production of new ones (at a certain distance). This happens due to the fact that the interactions effectively shift the atomic levels. Therefore, if the broadening of the latter induced by dissipation becomes comparable with the shift itself (e.g., $\Gamma \approx V$), the facilitation effect disappears and so does the critical behavior.

VI. CONCLUSIONS

In this work we have illustrated a number of nonequilibrium phenomena that can be explored within lattice gases of Rydberg atoms in the presence of local loss and gain processes. As a matter of fact, the latter, which are often regarded as unwanted sources of noise to overcome, turned out to be key for the emergence of the collective dynamics reported above. We remark that their presence constitutes a fundamental element

in our frame of thought. In the coarse-grained description employed here for the classical subspace, it is their interplay with the laser driving that determines the dynamical features highlighted.

In the limit of strong dephasing the Rydberg gas realizes several instances of transitions from and to absorbing states. Facilitating the flipping of atoms which possess a single excited neighbor yields a continuous transition whose dynamic properties vary smoothly depending on the average density of active sites, while the static ones remain unchanged. This is strongly reminiscent of the behavior of stochastic processes with multiple absorbing states. On the other hand, on a triangular lattice and with a resonance condition asking for two neighbors to be excited, the system undergoes a discontinuous phase transition, highlighted by the bimodal structure of the stationary density of excitations.

In the limit where the coherent laser excitation dominates the dephasing processes the static and dynamical properties of the system are determined by an equilibrium critical point belonging to the model A universality class. This hints at the possibility of investigating these collective behaviors in a setting complementary to the ones in which these phenomena were previously studied, all of which relied on the presence of radiative decay.

A particularly appealing aspect of the present study is the prospect to explore nonequilibrium phase transitions with absorbing states. Although the underlying universality classes—all of which relate, to a certain degree, to directed percolation—have been thoroughly investigated in the past, there are not many condensed-matter systems which are known to display the corresponding critical behaviors [70–72]. Rydberg gases in the presence of local loss and gain permit the detailed exploration of directed percolation universality in all three dimensions [32] and also in the presence of a manifold of absorbing states. Peculiar features such as the dependence of the critical dynamics on the initial state, which have been studied in the framework of idealized model systems, can now be in principle explored experimentally. Additionally, this setting opens the possibility to experimentally study the influence of quantum effects on the stochastic nonequilibrium processes.

ACKNOWLEDGMENTS

The authors would like to acknowledge R. Gutierrez and E. Levi for useful discussions. We are thankful for access to the University of Nottingham High Performance Computing Facility. The research leading to these results has received funding from the European Research Council under the European Union’s Seventh Framework Programme (FP/2007-2013)/ERC Grant Agreement No. 335266 (ESCQUIMA). Further funding was received through the H2020-FETPROACT-2014 Grant No. 640378 (RYSQ) and the EU-FET Grant No. 612862 (HAIRS). We also acknowledge financial support from EPSRC Grant No. EP/J009776/1.

-
- [1] I. Bloch, J. Dalibard, and W. Zwerger, Many-body physics with ultracold gases, *Rev. Mod. Phys.* **80**, 885 (2008).
 [2] R. Löw, H. Weimer, J. Nipper, J. B. Balewski, B. Butscher, H. P. Büchler, and T. Pfau, An experimental and theoretical guide

to strongly interacting Rydberg gases, *J. Phys. B* **45**, 113001 (2012).

- [3] T. F. Gallagher, *Rydberg Atoms* (Cambridge University Press, New York, 1984).

- [4] A. W. Carr and M. Saffman, Preparation of Entangled and Antiferromagnetic States by Dissipative Rydberg Pumping, *Phys. Rev. Lett.* **111**, 033607 (2013).
- [5] M. Ebert, M. Kwon, T. G. Walker, and M. Saffman, Coherence and Rydberg Blockade of Atomic Ensemble Qubits, *Phys. Rev. Lett.* **115**, 093601 (2015).
- [6] K. M. Maller, M. T. Lichtman, T. Xia, Y. Sun, M. J. Piotrowicz, A. W. Carr, L. Isenhower, and M. Saffman, A Rydberg blockade CNOT gate and entanglement in a 2D array of neutral atom qubits, *Phys. Rev. A* **92**, 022336 (2015).
- [7] H. Weimer, R. Löw, T. Pfau, and H. P. Büchler, Quantum Critical Behavior in Strongly Interacting Rydberg gases, *Phys. Rev. Lett.* **101**, 250601 (2008).
- [8] H. Weimer and H. P. Büchler, Two-stage Melting in Systems of Strongly Interacting Rydberg Atoms, *Phys. Rev. Lett.* **105**, 230403 (2010).
- [9] E. Levi, J. Minář, J. P. Garrahan, and I. Lesanovsky, Crystalline Structures and frustration in a two-component Rydberg gas, *New J. Phys.* **17**, 123017 (2015).
- [10] Y. O. Dudin, L. Li, F. Bariani, and A. Kuzmich, Observation of coherent many-body rabi oscillations, *Nat. Phys.* **8**, 790 (2012).
- [11] D. Barredo, S. Ravets, H. Labuhn, L. Béguin, A. Vernier, F. Nogrette, T. Lahaye, and A. Browaeys, Demonstration of a Strong Rydberg Blockade in Three-atom Systems with Anisotropic Interactions, *Phys. Rev. Lett.* **112**, 183002 (2014).
- [12] J. Zeiher, P. Schauß, S. Hild, T. Macrì, I. Bloch, and C. Gross, Microscopy of a Scalable Superatom, *Phys. Rev. X* **5**, 031015 (2015).
- [13] C. Ates, J. P. Garrahan, and I. Lesanovsky, Thermalization of a Strongly Interacting Closed Spin System: From Coherent Many-body Dynamics to a Fokker-Planck Equation, *Phys. Rev. Lett.* **108**, 110603 (2012).
- [14] S. Ji, C. Ates, J. P. Garrahan, and I. Lesanovsky, Equilibration of quantum hard rods in one dimension, *J. Stat. Mech.: Theory Exp.* (2013) P02005.
- [15] P. Schauß, M. Cheneau, M. Endres, T. Fukuhara, S. Hild, A. Omran, T. Pohl, C. Gross, S. Kuhr, and I. Bloch, Observation of spatially ordered structures in a two-dimensional Rydberg gas, *Nature (London)* **491**, 87 (2012).
- [16] M. Gärtner, K. P. Heeg, T. Gasenzer, and J. Evers, Dynamic formation of Rydberg aggregates at off-resonant excitation, *Phys. Rev. A* **88**, 043410 (2013).
- [17] H. Schempp, G. Günter, M. Robert-de-Saint-Vincent, C. S. Hofmann, D. Breyel, A. Komnik, D. W. Schönleber, M. Gärtner, J. Evers, S. Whitlock, and M. Weidemüller, Full Counting Statistics of Laser Excited Rydberg Aggregates in a One-Dimensional Geometry, *Phys. Rev. Lett.* **112**, 013002 (2014).
- [18] I. Lesanovsky and J. P. Garrahan, Kinetic Constraints, Hierarchical relaxation, and Onset of Glassiness in Strongly Interacting and Dissipative Rydberg Gases, *Phys. Rev. Lett.* **111**, 215305 (2013).
- [19] I. Lesanovsky and J. P. Garrahan, Out-of-equilibrium structures in strongly interacting Rydberg gases with dissipation, *Phys. Rev. A* **90**, 011603 (2014).
- [20] A. Urvoy, F. Ripka, I. Lesanovsky, D. Booth, J. P. Shaffer, T. Pfau, and R. Löw, Strongly Correlated Growth of Rydberg Aggregates in a Vapor Cell, *Phys. Rev. Lett.* **114**, 203002 (2015).
- [21] M. Mattioli, A. W. Glaetzle, and W. Lechner, From classical to quantum non-equilibrium dynamics of Rydberg excitations in optical lattices, *New J. Phys.* **17**, 113039 (2015).
- [22] M. Hoening, W. Abdussalam, M. Fleischhauer, and T. Pohl, Antiferromagnetic long-range order in dissipative Rydberg lattices, *Phys. Rev. A* **90**, 021603 (2014).
- [23] M. Höning, D. Muth, D. Petrosyan, and M. Fleischhauer, Steady-state crystallization of Rydberg excitations in an optically driven lattice gas, *Phys. Rev. A* **87**, 023401 (2013).
- [24] T. E. Lee, H. Häffner, and M. C. Cross, Antiferromagnetic phase transition in a nonequilibrium lattice of Rydberg atoms, *Phys. Rev. A* **84**, 031402 (2011).
- [25] C. Ates, B. Olmos, J. P. Garrahan, and I. Lesanovsky, Dynamical phases and intermittency of the dissipative quantum ising model, *Phys. Rev. A* **85**, 043620 (2012).
- [26] T. E. Lee, H. Häffner, and M. C. Cross, Collective Quantum Jumps of Rydberg Atoms, *Phys. Rev. Lett.* **108**, 023602 (2012).
- [27] C. Carr, R. Ritter, C. G. Wade, C. S. Adams, and K. J. Weatherill, Nonequilibrium Phase Transition in a Dilute Rydberg Ensemble, *Phys. Rev. Lett.* **111**, 113901 (2013).
- [28] M. Marcuzzi, E. Levi, S. Diehl, J. P. Garrahan, and I. Lesanovsky, Universal Nonequilibrium Properties of Dissipative Rydberg Gases, *Phys. Rev. Lett.* **113**, 210401 (2014).
- [29] H. Weimer, Variational Principle for Steady States of Dissipative Quantum Many-Body Systems, *Phys. Rev. Lett.* **114**, 040402 (2015).
- [30] H. Weimer, Variational analysis of driven-dissipative Rydberg gases, *Phys. Rev. A* **91**, 063401 (2015).
- [31] N. Malossi, M. M. Valado, S. Scotto, P. Huillery, P. Pillet, D. Ciampini, E. Arimondo, and O. Morsch, Full Counting Statistics and Phase Diagram of a Dissipative Rydberg Gas, *Phys. Rev. Lett.* **113**, 023006 (2014).
- [32] M. Marcuzzi, E. Levi, W. Li, J. P. Garrahan, B. Olmos, and I. Lesanovsky, Non-equilibrium universality in the dynamics of dissipative cold atomic gases, *New J. Phys.* **17**, 072003 (2015).
- [33] R. M. W. van Bijnen, C. Ravensbergen, D. J. Bakker, G. J. Dijk, S. J. J. M. F. Kokkelmans, and E. J. D. Vredenbregt, Patterned Rydberg excitation and ionization with a spatial light modulator, *New J. Phys.* **17**, 023045 (2015).
- [34] H. Hinrichsen, Non-equilibrium critical phenomena and phase transitions into absorbing states, *Adv. Phys.* **49**, 815 (2000).
- [35] F. Nogrette, H. Labuhn, S. Ravets, D. Barredo, L. Béguin, A. Vernier, T. Lahaye, and A. Browaeys, Single-Atom Trapping in Holographic 2D Arrays of Microtraps with Arbitrary Geometries, *Phys. Rev. X* **4**, 021034 (2014).
- [36] T. Wilk, A. Gaëtan, C. Evellin, J. Wolters, Y. Miroshnychenko, P. Grangier, and A. Browaeys, Entanglement of Two Individual Neutral Atoms Using Rydberg Blockade, *Phys. Rev. Lett.* **104**, 010502 (2010).
- [37] D. Barredo, H. Labuhn, S. Ravets, T. Lahaye, A. Browaeys, and C. S. Adams, Coherent Excitation Transfer in a Spin Chain of Three Rydberg Atoms, *Phys. Rev. Lett.* **114**, 113002 (2015).
- [38] A. Gaëtan, Y. Miroshnychenko, T. Wilk, A. Chotia, M. Viteau, D. Comparat, P. Pillet, A. Browaeys, and P. Grangier, Observation of collective excitation of two individual atoms in the Rydberg blockade regime, *Nat. Phys.* **5**, 115 (2009).
- [39] M. Marcuzzi, J. Schick, B. Olmos, and I. Lesanovsky, Effective dynamics of strongly dissipative Rydberg gases, *J. Phys. A* **47**, 482001 (2014).
- [40] N. Schlosser, G. Reymond, I. Protsenko, and P. Grangier, Subpoissonian loading of single atoms in a microscopic dipole trap, *Nature (London)* **411**, 1024 (2001).

- [41] N. Schlosser, G. Reymond, and P. Grangier, Collisional Blockade in Microscopic Optical Dipole Traps, *Phys. Rev. Lett.* **89**, 023005 (2002).
- [42] M. D. Lukin, M. Fleischhauer, R. Cote, L. M. Duan, D. Jaksch, J. I. Cirac, and P. Zoller, Dipole Blockade and Quantum Information Processing in Mesoscopic Atomic Ensembles, *Phys. Rev. Lett.* **87**, 037901 (2001).
- [43] E. Urban, T. A. Johnson, T. Henage, L. Isenhower, D. D. Yavuz, T. G. Walker, and M. Saffman, Observation of Rydberg blockade between two atoms, *Nat. Phys.* **5**, 110 (2009).
- [44] F. W. Cummings and A. Dorri, Exact solution for spontaneous emission in the presence of n atoms, *Phys. Rev. A* **28**, 2282 (1983).
- [45] U. Raitzsch, R. Heidemann, H. Weimer, B. Butscher, P. Kollmann, R. Löw, H. P. Büchler, and T. Pfau, Investigation of dephasing rates in an interacting Rydberg gas, *New J. Phys.* **11**, 055014 (2009).
- [46] G. Lindblad, On the generators of quantum dynamical semi-groups, *Commun. Math. Phys.* **48**, 119 (1976).
- [47] H. P. Breuer and F. Petruccione, *The Theory of Open Quantum Systems* (Oxford University Press, New York, 2007).
- [48] C. Ates, T. Pohl, T. Pattard, and J. M. Rost, Strong interaction effects on the atom counting statistics of ultracold Rydberg gases, *J. Phys. B* **39**, L233 (2006).
- [49] K. P. Heeg, M. Gärtner, and J. Evers, Hybrid model for Rydberg gases including exact two-body correlations, *Phys. Rev. A* **86**, 063421 (2012).
- [50] S. Nakajima, On quantum theory of transport phenomena: Steady diffusion, *Prog. Theor. Phys.* **20**, 948 (1958).
- [51] R. Zwanzig, Ensemble method in the theory of irreversibility, *J. Chem. Phys.* **33**, 1338 (1960).
- [52] P. Degenfeld-Schonburg and M. J. Hartmann, Self-consistent projection operator theory for quantum many-body systems, *Phys. Rev. B* **89**, 245108 (2014).
- [53] G. Ódor, Universality classes in nonequilibrium lattice systems, *Rev. Mod. Phys.* **76**, 663 (2004).
- [54] H. Hinrichsen, M. Henkel and S. Lübeck, *Non-Equilibrium Phase Transitions*, Theoretical and Mathematical Physics Vol. 1 (Springer Netherlands, Dordrecht, 2009).
- [55] G. S. Agarwal, Open quantum Markovian systems and the microreversibility, *Z. Phys.* **258**, 409 (1973).
- [56] R. Chetrite and K. Mallick, Quantum fluctuation relations for the Lindblad master equation, *J. Stat. Phys.* **148**, 480 (2012).
- [57] C. Aron, G. Biroli, and L. F. Cugliandolo, Symmetries of generating functionals of Langevin processes with colored multiplicative noise, *J. Stat. Mech.* (2010) P11018.
- [58] L. M. Sieberer, A. Chiocchetta, A. Gambassi, U. C. Täuber, and S. Diehl, Thermodynamic Equilibrium as a Symmetry of the Schwinger-Keldysh Action, *Phys. Rev. B* **92**, 134307 (2015).
- [59] Z. Racz, Nonequilibrium Phase Transitions, [arXiv:cond-mat/0210435](https://arxiv.org/abs/cond-mat/0210435).
- [60] I. Jensen and R. Dickman, Nonequilibrium phase transitions in systems with infinitely many absorbing states, *Phys. Rev. E* **48**, 1710 (1993).
- [61] J. F. F. Mendes, R. Dickman, M. Henkel, and M. C. Marques, Generalized scaling for models with multiple absorbing states, *J. Phys. A* **27**, 3019 (1994).
- [62] P. Grassberger, H. Chaté, and G. Rousseau, Spreading in media with long-time memory, *Phys. Rev. E* **55**, 2488 (1997).
- [63] D. Petrosyan and K. Mølmer, Binding Potentials and Interaction Gates Between Microwave-Dressed Rydberg Atoms, *Phys. Rev. Lett.* **113**, 123003 (2014).
- [64] M. Kiffner, W. Li, and D. Jaksch, Three-Body Bound States in Dipole-Dipole Interacting Rydberg Atoms, *Phys. Rev. Lett.* **111**, 233003 (2013).
- [65] M. Kiffner, W. Li, and D. Jaksch, Magnetic Monopoles and Synthetic Spin-Orbit Coupling in Rydberg Macrodimers, *Phys. Rev. Lett.* **110**, 170402 (2013).
- [66] S. H. Strogatz, *Nonlinear Dynamics and Chaos: With Applications to Physics, Biology, Chemistry, and Engineering*, Advanced Book Program (Westview Press, Boulder, CO, 1994).
- [67] A. Hu, T. E. Lee, and C. W. Clark, Spatial correlations of one-dimensional driven-dissipative systems of Rydberg atoms, *Phys. Rev. A* **88**, 053627 (2013).
- [68] J. Jin, D. Rossini, R. Fazio, M. Leib, and M. J. Hartmann, Photon Solid Phases in Driven Arrays of Nonlinearly Coupled Cavities, *Phys. Rev. Lett.* **110**, 163605 (2013).
- [69] P. C. Hohenberg and B. I. Halperin, Theory of dynamic critical phenomena, *Rev. Mod. Phys.* **49**, 435 (1977).
- [70] H. Hinrichsen, On possible experimental realizations of directed percolation, *Braz. J. Phys.* **30**, 69 (2000).
- [71] K. A. Takeuchi, M. Kuroda, H. Chaté, and M. Sano, Directed Percolation Criticality in Turbulent Liquid Crystals, *Phys. Rev. Lett.* **99**, 234503 (2007).
- [72] K. A. Takeuchi, M. Kuroda, H. Chaté, and M. Sano, Experimental realization of directed percolation criticality in turbulent liquid crystals, *Phys. Rev. E* **80**, 051116 (2009).